Computer-Assisted Motion Analysis of Neuronal Cell Growth

STACY S. HAWKINS,[1,2,*] HELEN M. BUETTNER,[1] STANLEY M. DUNN[2]

[1]Department of Chemical and Biochemical Engineering, Rutgers University, Piscataway, New Jersey 08855-0909

[2]Department of Biomedical Engineering, Rutgers University, Piscataway, New Jersey 08855-0909

Received 24 July 1995; accepted 16 May 1995

ABSTRACT: Characterization of neuronal cell growth provides key information about the development of neural pathways during embryogenesis as well as their regeneration following postnatal nerve injury. However, very active cell types like growing neurons are difficult to track in detail because their motion is complex and cellular features have a tendency to move out of the focal plane or occlude one another. Due to these difficulties, characterization of neuronal growth dynamics has been less quantitative than desired. To address this problem, we developed a method for the automated motion analysis of neuronal growth based on image analysis and shape correspondence techniques. This method increases the rate at which we can obtain dynamic data by at least an order of magnitude. We focus specifically on the *growth cone,* a specialized, cell-like structure at the growing neurite tip whose behavior is believed to be a key determinant of neuronal growth. © 1997 John Wiley & Sons, Inc. J Appl Polym Sci **63:** 1413–1422, 1997

Key words: nerve growth dynamics; nerve regeneration; growth cone; computer vision; image analysis

INTRODUCTION

The ability to predict and control neuronal growth in both biological and biosynthetic environments represents a critical step in the tissue engineering of neural systems. Specific applications include the improved repair of injured nerves, the development of *in vitro* neural networks, and the construction of bioartificial devices.[1] A lack of quantitative data has, however, made this an elusive goal. Neuronal growth occurs *in vivo* and *in vitro* by the guided extension of neurites (axons and dendrites) from the neuronal cell body, a process regulated by the *growth cone.*[2] The growth cone is a motile expansion at the neurite tip (see Fig. 1) that displays a dynamic morphology, changing shape rapidly and apparently randomly in both time and space. While the dynamics of this continual and complex remodeling are believed to hold many clues to the underlying mechanisms of neurite growth, they have proven quite difficult to track. In addition, the small size of growth cone features (ranging down to less than 1 micron) and the difficulties associated with staining live neurons leads to the use of high-resolution, phase contrast microscopy for most experimental observations of growth cone behavior and, consequently, images characterized by noise and low contrast. In this article, we present a method that greatly facilitates the tracking and analysis of neuronal growth cone morphology from such images. Because this represents a particularly challenging

Correspondence to: H. M. Buettner

** Present address:* Clinical and Appraisal Science, Unilever Research U.S., 45 River Road, Edgewater, NJ 07020

Contract grant sponsor: Whitaker Foundation

Contract grant sponsor: National Science Foundation

Contract grant number: BCS-9210540

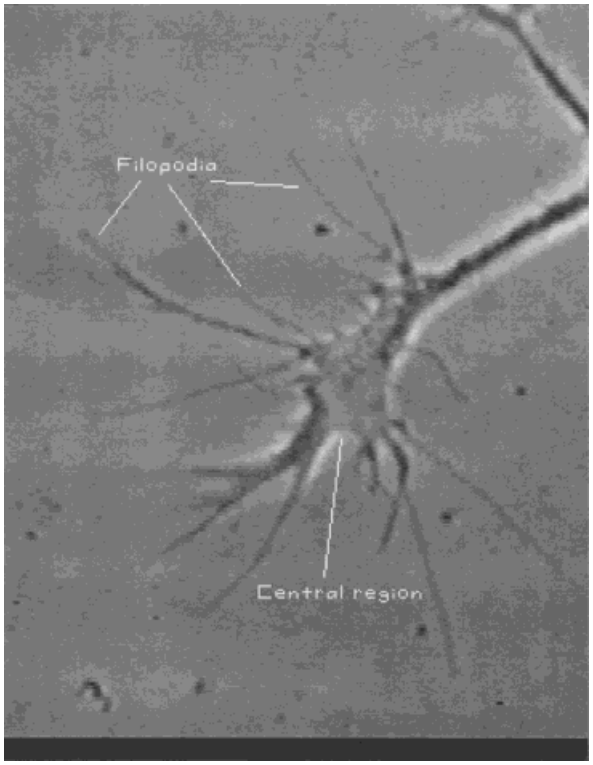

Figure 1 Growth cone from chick DRG neuron growing on a laminin-coated glass coverslip. Labeled modalities are the central region and filopodia.

problem in the analysis of cell motility, our method should be suitable for characterizing motion by many other cell types as well.

For purposes of analysis, the growth cone is often divided conceptually into two main regions of interest (Fig. 1):

1. The *central* region, which is relatively rounded and typically exhibits lamellipodial veils at its periphery.
2. The *filopodia,* which are longer, fingerlike structures projecting from the periphery of the lamellipodial region.

Both of these regions are important to neurite growth. Experiments in which the central region is deprived of filopodia by pharmacological treatment show that growth can continue in their absence but appears undirected,[3–5] suggesting that the central region may be primarily responsible for neurite extension with the filopodia playing a major role in growth cone guidance. In addition, pharmacological treatment leading to collapse of the central region causes the neurite to retract.[6]

From an image analysis perspective, the motion of the growth cone can be characterized as nonrigid, since the central region deforms and the filopodia extend, bend, retract, and eventually disappear. Three basic methods can be applied to analyze nonrigid motion:

1. *Differential geometry techniques,* in which the contour of an object is assumed to undergo conformal motion (see Fig. 2). Conformal motion preserves angles between curves, but not distances between points.[7–9]
2. *Overconstrained global descriptors,* which employ statistics or previous changes in a contour to predict future changes.[10–12]

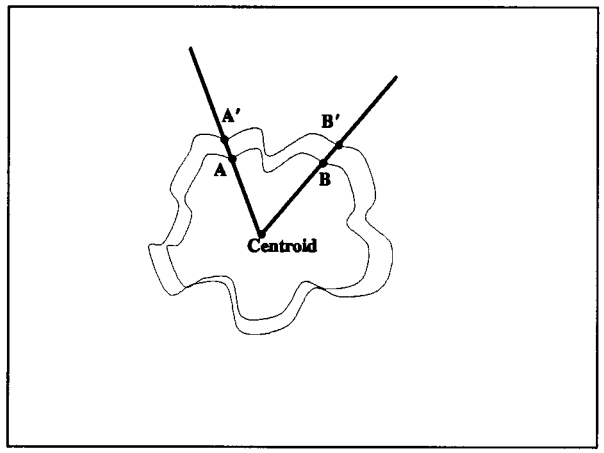

Figure 2 Example of conformal stretching. The two curves have the same centroid, and angles between points are preserved, but the degree of stretching in the x- and y-directions are different.

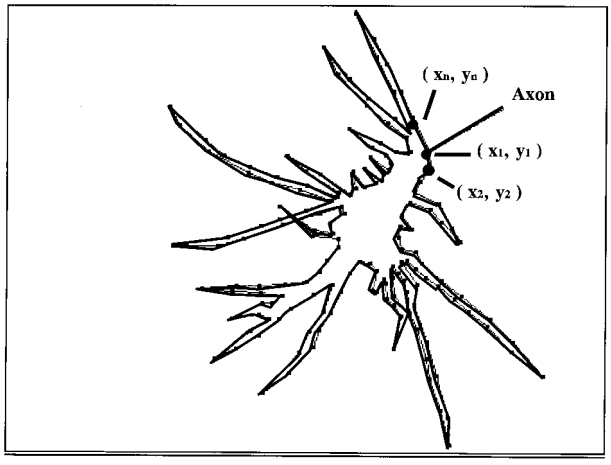

Figure 3 Outline of the growth cone in Figure 1, showing its contour as a series of connected straight line segments with points labeled in a clockwise manner.

3. *Energy-minimizing active contours,* where the contour of the object is defined as the region of minimal energy. The energy of the contour is defined as the sum of image contrast, image intensity, and smoothness constraints between contour points.[13–16] These techniques have been applied for segmenting pseudopods[17] and dendritic processes.[18]

The motion of the growth cone is difficult to track using differential geometry techniques for two significant reasons: First, growth cone motion cannot be classified as a constant stretching or deformation or other deterministic kinds of behavior. In addition, differential geometry techniques can be impractical when the images are very noisy or when the intensity of the object does not vary significantly from the background of the image, both of which occur here.

Overconstrained techniques could not be applied since there are no current statistics available to describe the motion of the growth cone features. In addition, features along the growth cone contour disappear as the filopodia retract and as the axon moves across the coverslip. For these reasons, our motion analysis is based on active contour techniques.

EXPERIMENTAL

Neuronal Cell Culture and Video Microscopy

Measurements were made on chick dorsal root ganglion (DRG) neurons obtained at embryonic day 7–8. The ganglia were placed on glass coverslips coated with laminin and incubated overnight at 37°C. Immediately prior to observation, the coverslips were affixed to microscope slides to form a sealed culture chamber. Individual neurites were then identified and tracked using time-lapse video microscopy. Cultures were filmed at a constant temperature (37°C) on the incubated stage of a Leitz Labovert inverted microscope. Microscopy was performed using a 100× oil immersion phase contrast objective, a 1.6× projection lens, and a Dage MTI pasecon video camera. A Macintosh IIci equipped with a RasterOps 24STV frame grabber was used to grab digital video sequences at a rate of 0.25 frames/s, which approached the lower limit on the time interval in which significant movement could be detected. The frames were stored on a 1.3 Gb hard drive prior to analysis and then archived on digital audiotape.

Two-dimensional Motion Analysis of the Growth Cone

Time-dependent characteristics of growth cone morphology were analyzed by first generating

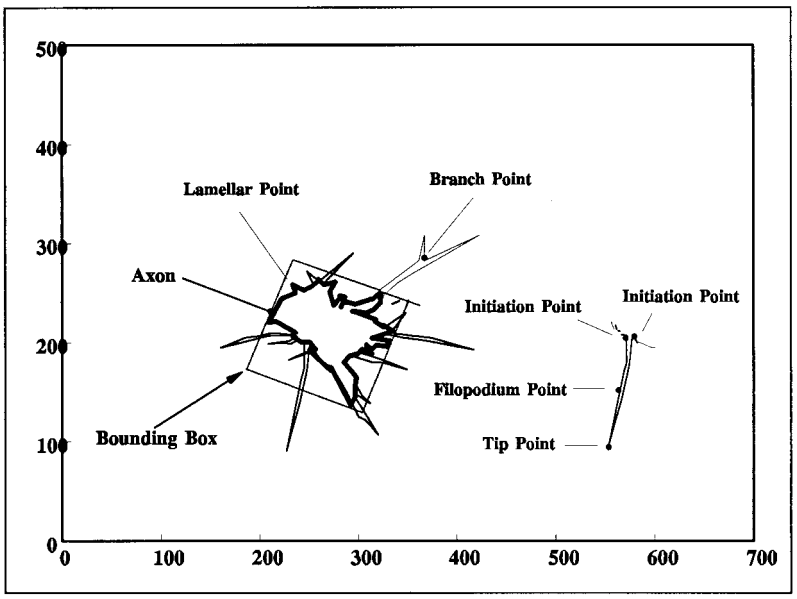

Figure 4 Axon, lamellipodium, filopodium, tip, initiation, and branch points. The filopodia are the spiky structures projecting from the central region. The bounding box of the central region, which represents the maximum extension parallel and perpendicular to the axon, is marked by the dotted line.

two-dimensional outlines of all the growth cone images in a video sequence. In this manner, only the lamellipodia and filopodia at the tip of the structure were measured. The axon position was recorded as the location where the central region first began to spread outward from the axon. These contours were produced either (1) by displaying the individual images of a sequence on a Sun Sparcstation running X-Windows and outlining the growth cone images manually as a series of connected straight-line segments (semiautomatic method) or (2) by deriving the contour automatically (fully automatic method). In each case, the contour was denoted as a set of N discrete points, $\nu(x_i, y_i)$, where $i = 1, 2, \cdots N$ (see Fig. 3). This approximates a continuous contour denoted by $\nu(s) = [x(s), y(s)]$, with first and second derivatives $\nu_s(s)$ and $\nu_{ss}(s)$, where s is the normalized arc length, defined as the ratio of the distance along the contour divided by the total contour length. Algorithms for both manual and computer-automated outlining, as well as subsequent tracking of morphological features within a sequence of outlines, were written in the C programming language and run on a Sun Sparcstation.

Contours were derived automatically using active contour techniques. These techniques interpret the sequence of outlines as a two-dimensional active contour, or *snake,* composed of elastic components—strings, which permit creases or folds, and rods, which are resistant to bending and tend to smooth the contour. The snake "locks on" to a contour in an image when its energy is minimized, as determined by image forces, smoothness con-

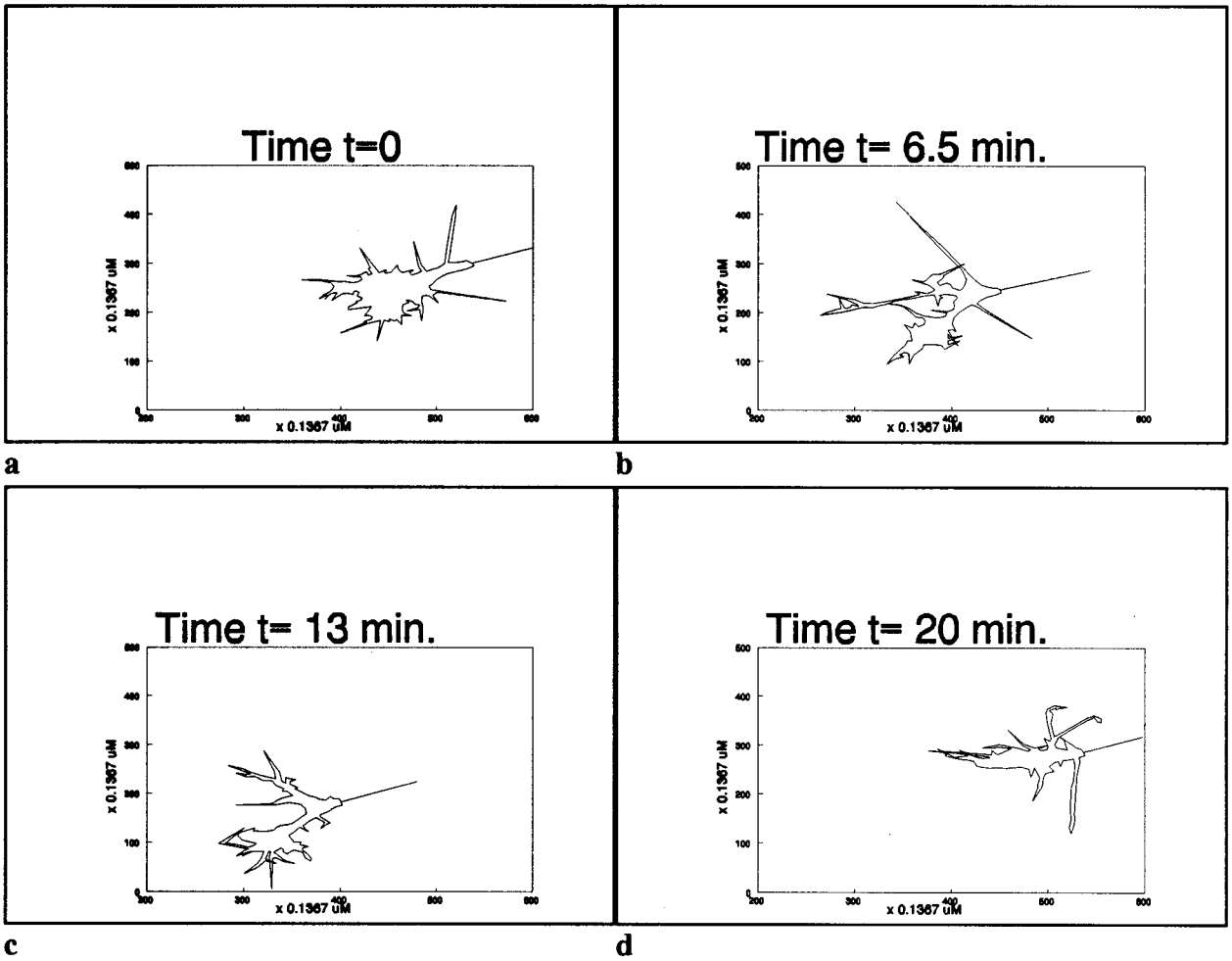

Figure 5 Outlines of actual chick DRG growth cone contours in a time series: (a) time = 0 min; (b) time = 6.5 min; (c) time = 13 min; (d) time = 20 min. The lack of a conserved structure between contours illustrates that the growth cone does not exhibit conformal stretching/deformation.

straints, and user-defined external constraints. For example, movement of one of the points toward salient features in the image, such as dark patches, will result in lowering the energy of the contour (for a detailed description, see the Appendix).

Sequences of chick DRG growth cone motion used for this analysis were processed either semiautomatically or fully automatically by computer and then verified manually for comparison. The user was prompted to segment the contours manually or automatically using the deformable contour models described above.[19,20] In the fully automatic case, feature points were added as the contour expanded during filopodial or lamellipodial extension and removed during filopodial retraction or lamellipodial contraction (by a computer-driven algorithm). We used a discrete, multistage decision process for extracting the contours of the growth cone in the fully automatic case. The elasticity, or pulling force exerted between points, was determined by the position of the point along the contour, or point label, as described in the following section.[19,20]

RESULTS

Automatic Labeling and Tracking

The primary result of this work is a motion analysis system which we refer to as SEaLNeT (*S*urface *E*xtraction *a*nd *L*abeling for *N*eurite *T*racking), for tracking morphological features of the motile growth cone from a series of growth cone contours. Using SEaLNeT, the points in each contour are automatically assigned feature labels based on the curvature of the contour at the given point; these features are then tracked and analyzed without user intervention for the sequence of images.

The assigned point labels are dependent on a local neighborhood of other points. The curvature, k_i, of a point, i, is defined by

$$k_i = \frac{dx_i}{ds}\frac{d^2y_i}{ds^2} - \frac{dy_i}{ds}\frac{d^2x_i}{ds^2} \qquad (1)$$

The following set of rules is employed in identifying feature labels (see Fig. 4):

1. The axon point (point at which the axon shaft meets the growth cone) is the first point along the contour.
2. All points with very high positive (convex relative to the centroid) curvature are temporarily labeled as tip points.
3. Initiation points for these temporary points are then labeled based on the following criteria:

- Relatively high negative (concave relative to the centroid) curvature.

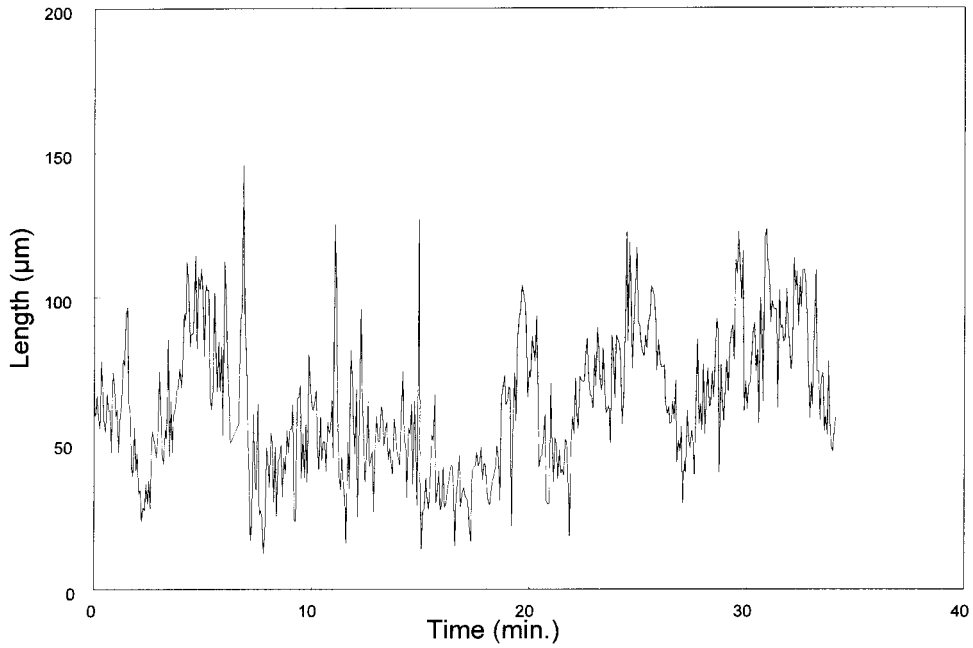

Figure 6 Time series of total filopodial length.

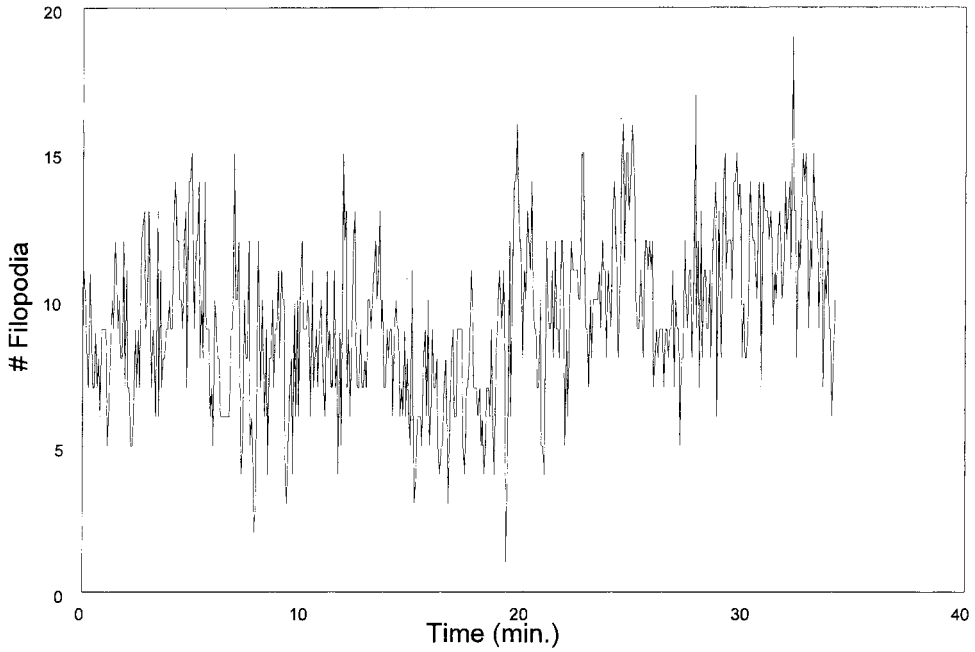

Figure 7 Time series of total filopodial number.

- Distance between initiation points for a corresponding tip point of a given filopodium is small.
- The lengths between the initiation points and tip for a given filopodium are approximately equal.

4. The length-to-width ratios (distance between tip and initiation point vs. distance between initiation points for a given filopodium) are computed. All points that were previously labeled as tip and initiation points that do not have at least a length-to-width ratio of 2 : 1 are reset as points along the central region.
5. All points between initiation and tip points

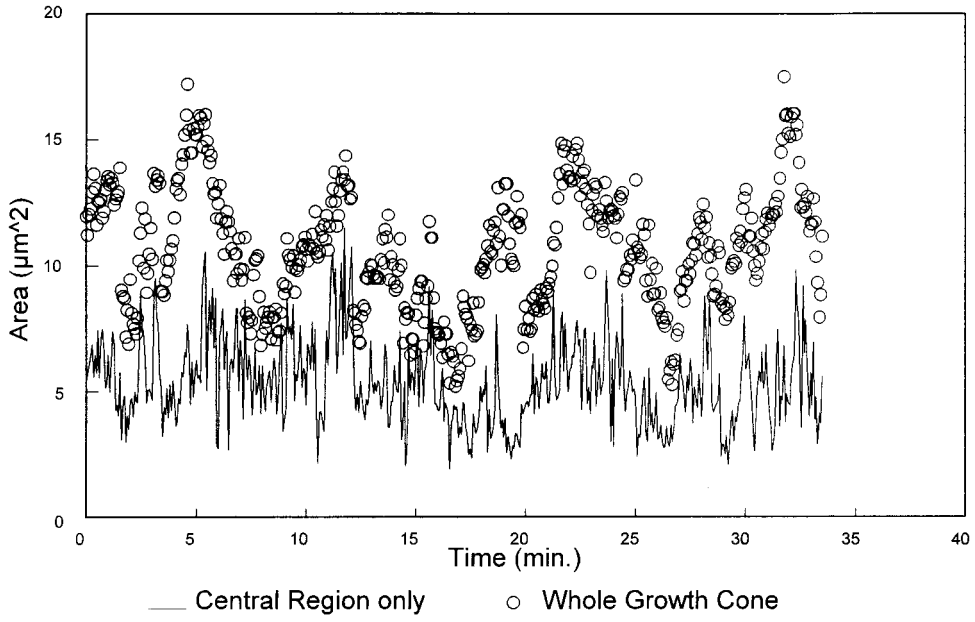

Figure 8 Area of the whole growth cone (central region and filopodia) compared to the area of the central region alone.

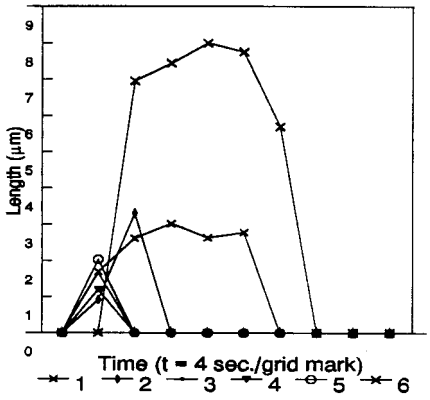

Figure 9 Summary of lifespans of first six newly initiating filopodia (length in μm vs. time).

that have very high negative curvature are labeled as branch points (where two separate filopodia have the same initiation point).

6. Central region points are labeled as all remaining points between the axon and initiation point or two initiation points.
7. Filopodium points are labeled as all remaining points between an initiation and tip point, an initiation and branch point, or a branch and tip point.

Several contours of a growth cone from a representative video sequence are shown in Figure 5. We performed semiautomatic motion analysis on numerous sequences to date, typically consisting of 200–1000 images. Computations are completed at a rate of several hundred frames per hour on a Sun Sparcstation 2, leading to an order of magnitude improvement in the overall rate of analysis when compared to nonautomated methods previously described.[21] Accuracy of the analysis was evaluated in terms of three key types of points: the centroid and the filopodial tip and initiation points. Labeling and measurement of all other features in a contour depend upon the correct identification of these three basic features. Agreement with visual identification of the same feature points by an expert was typically greater than 93%, with discrepancies occurring only in the case of blurred images or complex morphologies in which features were quite ambiguous.

Once the points along the growth cone contours are labeled, SEaLNeT computes the following quantitative information (see Fig. 4):

1. Total number of filopodia in a given frame.
2. Total length of all filopodia in a given frame.
3. Area of the central region and whole growth cone.
4. Angles of initiation and tip points and lengths for individual filopodia.
5. Bounding box or total extension of the central region.
6. Variance, standard deviation, skew, and kurtosis in x- and y-directions.
7. Axon and centroid angles and positions.

A time series of the total length and number of the filopodia in a given frame, the areas of the whole growth cone and the central region, and the lengths of the first six newly initiating filopodia are shown in Figures 6–9. The summary of the position and angle of the axon as it moved across the coverslip are shown in Figure 10(a) and (b), respectively.

Fully automatic processing reduced the total analysis time by a factor of 30 compared to manual processing; semiautomatic reduced the total analysis time by a factor of 10 when compared to manual processing. Manual processing can be completed at a rate of about five growth cones/day, requiring more than 1 month to acquire even a minimal data set for estimating dynamic characteristics of growth cone morphology. For sequences with less dynamic filopodial activity, the accuracy of automatic processing was greater than 95%. However, accuracy dropped significantly as behavior became more dynamic, making the fully automatic method useful only in specific cases. The choice of the appropriate method (fully or semiautomatic) depended on the experimental setup. The fully automatic method could always be applied to track the central region and axon in a homogeneous environment, but the semiautomatic method was applied the majority of the time when other contours (other axons or substrate borders) were present.

DISCUSSION

We have developed a method for computing quantitative information about the dynamic morphology of the growth cone. This system can be used in one of two ways:

1. *Semiautomatic operation*—Manual contour extraction with automatic feature labeling and motion tracking.
2. *Fully automatic operation*—Automatic con-

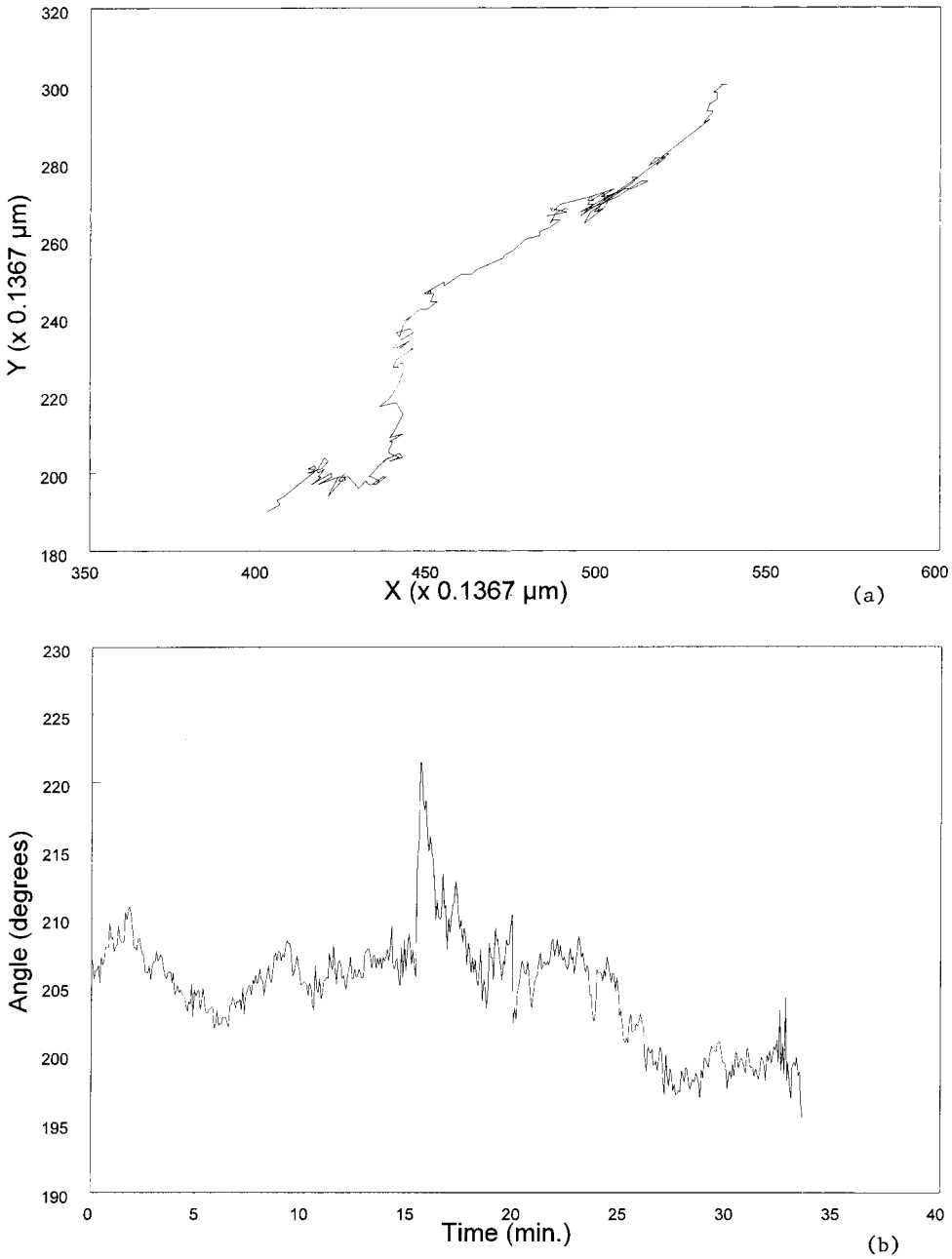

Figure 10 (a) Growth cone trajectory. The growth cone axon moved from the top right corner to the bottom left corner over a 30 min series. (b) Time series of axon angle.

tour extraction, feature labeling, and motion tracking.

The fully automatic operation tremendously increases the rate at which dynamic morphological data can be obtained on the complex structure of the growth cone. However, it cannot be used reliably for highly motile behavior. The semiautomatic method is accurate in all cases while providing a significant time savings, albeit less than the fully automatic method.

One long-term goal is to modify our image analysis system to permit the user to watch the contour extraction process and to move any incorrect points. The contour of the previous frame will be superimposed over the growth cone in the current

frame and then relax around the growth cone in the current frame (as described by the energy-minimizing deformable contours above). The user will then correct for errors in the overall contour by moving certain points or regions with the mouse. In addition, the user can view previously outlined frames with or without the growth cone outlines to aid in the determination of the overall contour. In this way, motion tracking will be highly accurate and user interaction will be minimized.

Future studies will include tracking the growth cone across different substrates and in the presence of other axons. Studies of the growth cone under varying environmental conditions are crucial to assess the role of each environmental factor and to aid in the overall process of nerve repair and guidance. Quantitative analysis of many separate recordings, such as the one described here, will be used as a base line for future studies where motion is measured under varying, inhomogeneous environments.

APPENDIX

The energy of the closed contour (snake) of s, E^*_{snake}, can be written as follows:

$$E^*_{snake} = \min \int_0^1 E_{snake}[\nu(s)]\, ds \quad \text{(A.1)}$$

$$= \min \int_0^1 \{E_{int}[\nu(s)] + E_{image}[\nu(s)] + E_{con}[\nu(s)]\}\, ds \quad \text{(A.2)}$$

where the energy describing the overall smoothness of contour s is given by

$$E_{int} = \frac{\alpha(s)|\nu_s(s)|^2 + \beta(s)|\nu_{ss}(s)|^2}{2} \quad \text{(A.3)}$$

E_{int}, E_{image}, and E_{con} represent the internal smoothness energy, image force energy, and external constraint energy of the contour, respectively. The first-order weight, α, constrains the contour to be like a membrane, and the second-order term, β, constrains the contour to be more like a thin plate. Image energy forces were represented here as

$$E_{\text{image}} = \omega_{\text{edge}} E_{\text{edge}} + \omega_{\text{intensity}} E_{\text{intensity}} \quad \text{(A.4)}$$

The sum of external constraint and image force energy was represented by

$$E_{\text{ext}} = E_{\text{image}} + E_{\text{con}} \quad \text{(A.5)}$$

and the partial derivatives were represented as

$$f_x(i) = \frac{\partial E_{\text{ext}}}{\partial x_i} \quad \text{(A.6)}$$

$$f_y(i) = \frac{\partial E_{\text{ext}}}{\partial y_i} \quad \text{(A.7)}$$

The discrete representation of internal forces, E_{int}, for point i was given as

$$\begin{aligned} &\alpha_i(\nu_i - \nu_{i-1}) - \alpha_{i+1}(\nu_{i+1} - \nu_i) \\ &\quad + \beta_{i-1}(\nu_{i-2} - 2\nu_{i-1} + \nu_i) \\ &\quad - 2\beta_i(\nu_{i-1} - 2\nu_i + \nu_{i+1}) \\ &\quad + \beta_{i+1}(\nu_i - 2\nu_{i+1} + \nu_{i+2}) \end{aligned} \quad \text{(A.8)}$$

The energy of the entire system of points can be found by forming a system of equations for all points along the contour:

$$A_x + f_x(x, y) = 0 \quad \text{(A.9)}$$

$$A_y = f_y(x, y) = 0 \quad \text{(A.10)}$$

where A is a matrix formed by rows of elasticity constraints described for each point in terms of α and β, described above. These equations can be solved iteratively with

$$x_t = (A + \gamma I)^{-1}[x_{t-1} - f_x(x_{t-1}, y_{t-1})] \quad \text{(A.11)}$$

$$y_t = (A + \gamma I)^{-1}[y_{t-1} - f_y(x_{t-1}, y_{t-1})] \quad \text{(A.12)}$$

where γ denotes step size. Terzopoulos and Szeliski[16] proposed adding an inertial term to the external energy to prevent the snake from deforming too much when the image sequence becomes distorted or out of focus. This term is useful for tracking motion in objects where small deformations are anticipated. However, this term was not used for our calculations since shape changes could be very large and constraining our contour model to permit only small deformations resulted in inaccurate tracking.

This research was supported by grants from the Whitaker Foundation and NSF BCS-9210540 to H.M.B.

REFERENCES

1. A. Curtis, L. Breckenridge, P. Connolly, J. Dow, C. Wilkinson, and R. Wilson, *Med. Biol. Eng. Comput.,* **30,** CE33–CE36 (1992).
2. B. Alberts, D. Bray, J. Lewis, M. Raff, K. Roberts, and J. D. Watson, *Molecular Biology of the Cell,* 3rd ed., Garland, New York, 1994.
3. D. Bentley and A. Toroian-Raymond, *Nature,* **323,** 712–715 (1986).
4. C. Chien, D. Rosenthal, W. Harris, and C. Holt, *Neuron,* **11,** 237–251 (1993).
5. L. Marsh and P. Letourneau, *J. Cell Biol.,* **99,** 2041–2047 (1984).
6. J. Bamburg, D. Bray, and K. Chapman, *Nature,* **321,** 788–790 (1986).
7. A. Amini and J. Duncan, in *Proceedings IEEE Workshop on Visual Motion,* 1991, pp. 294–299.
8. D. Goldgof, H. Lee, and T. Huang, in *IEEE Computer Society Conference on Computer Vision and Pattern Recognition,* 1988, pp. 375–380.
9. C. Kambhamettu and D. Goldgof, in *IEEE Computer Society Conference on Computer Vision and Pattern Recognition,* 1992, pp. 222–227.
10. L. Cohen and I. Cohen, *IEEE Trans. Pattern Anal. Mach. Intel.,* **15**(11), 1131–1147 (1993).
11. A. Pentland, B. Horowitz, and S. Sclaroff, in *Proceedings IEEE Workshop on Visual Motion,* 1991, pp. 288–293.
12. A. Young and L. Axel, in *IEEE Computer Society Conference on Computer Vision and Pattern Recognition,* 1992, pp. 399–404.
13. M. Kass, A. Witkin, and D. Terzopoulos, in *Proceedings IEEE First International Conference on Computer Vision,* 1987, pp. 259–268.
14. T. Poggio, V. Torre, and C. Koch, *Nature,* **317,** 314–319 (1985).
15. D. Terzopoulos, *IEEE Trans. Pattern Anal. Mach. Intell.,* **8**(4), 413–423 (1986).
16. D. Terzopoulos and R. Szeliski, in *Active Vision,* A. Blake and A. Yuille, Eds., MIT Press, Cambridge, MA, pp. 3–20.
17. F. Leymarie and M. Levine, *IEEE Trans. PAMI,* **15**(6), 617–634 (1993).
18. I. Carlbom, D. Terzopoulos, and K. Harris, in *Scientific Visualization of Physical Phenomena,* N. M. Patrikalakis, Ed., Springer-Verlag, Heidelberg, 1991, pp. 623–638.
19. S. Hawkins-Gwydir, PhD Thesis, Rutgers University, May 1994.
20. S. Hawkins-Gwydir, H. Buettner, and S. Dunn, in *Proceedings of the IEEE Workshop on Biomedical Image Analysis,* 1994, pp. 80–87.
21. H. Buettner, R. Pittman, and J. Ivins, *Dev. Biol.,* **163,** 407–422 (1994).